

Computing Hydrogen Tunneling Splittings with Nuclear-Electronic Orbital Multireference Configuration Interaction

Rachel J. Stein, Christopher L. Malbon, and Sharon Hammes-Schiffer*

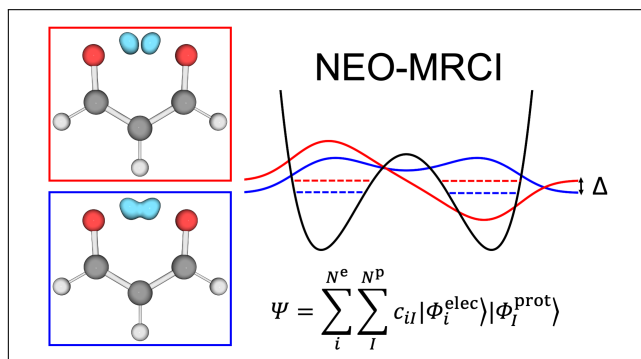
Department of Chemistry, Princeton University, Princeton, NJ 08544

E-mail: shs566@princeton.edu

Abstract

Hydrogen tunneling is an important process that impacts reaction rates and molecular spectra. Describing and understanding this process requires a quantum mechanical treatment of the transferring hydrogen. The nuclear-electronic orbital (NEO) approach treats specified nuclei quantum mechanically on the same level as electrons and has recently been implemented at the multireference configuration interaction (MRCI) wavefunction level. The NEO-MRCI method includes both the static correlation necessary to describe hydrogen tunneling and the electron-proton dynamic correlation required for computing quantitatively accurate nuclear-electronic vibronic states. Herein, the NEO-MRCI method is used to compute the nuclear-electronic wavefunctions and corresponding vibronic energies for four hydrogen tunneling systems at fixed geometries for a range of donor-acceptor distances. Comparison of the NEO-MRCI results to numerically exact grid-based calculations shows that the NEO-MRCI method can be used to obtain accurate hydrogen and deuterium tunneling splittings. Thus, this work presents an effective method for studying hydrogen tunneling systems.

TOC Graphic



Hydrogen tunneling and proton transfer play important roles in a wide range of chemical processes in molecular, biological, and electrochemical systems. A prime example is the prevalence of hydrogen tunneling in proton-coupled electron transfer (PCET) in enzymatic and electrocatalytic¹⁻⁸ reactions. Hydrogen tunneling splittings can be measured spectroscopically,⁹⁻¹² providing information about the structural and dynamical properties. Additionally, hydrogen isotope effects on tunneling splittings can offer valuable insights into reaction mechanisms.¹³⁻¹⁶ The ground state tunneling splitting is typically defined as the energy difference between the lowest two vibronic states corresponding to symmetric and antisymmetric bilobal wavefunctions (Fig. 1). For electronically adiabatic systems, these two vibronic states correspond to the lowest two proton vibrational states on the electronic ground state, where the proton is moving on a symmetric (or nearly symmetric) double-well potential energy surface. Given the widespread importance of hydrogen tunneling and the sensitivity of tunneling to the underlying potential energy surface, the development of high-level theoretical methods to compute precise proton vibrational wavefunctions, accurate tunneling splittings, and isotope effects is desirable.

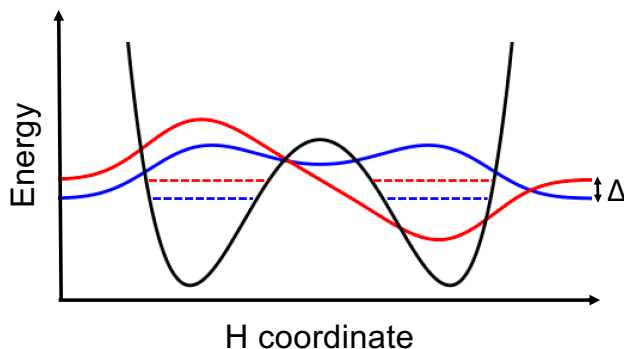


Figure 1. Schematic one-dimensional double-well proton potential energy profile and associated symmetric (blue) and antisymmetric (red) proton vibrational wavefunctions with vibrational state energies indicated by dotted lines. The tunneling splitting, Δ , is the difference in energy between these two vibrational states. This one-dimensional picture is for visualization purposes; all tunneling splitting calculations in this work were calculated in three dimensions.

The calculation of tunneling splittings is notoriously challenging. These splittings depend strongly on the electronic potential energy surface, especially the width and height of the tunneling barrier. An accurate description of hydrogen tunneling requires the incorporation of the nuclear

quantum effects of the tunneling proton and its coupling to the electronic wavefunction. A wide range of theoretical methods have been developed to model tunneling processes, such as path integral methods,^{17–19} diffusion Monte Carlo,^{20–23} and the multiconfiguration time-dependent Hartree approach.^{24–26} The nuclear-electronic orbital (NEO) approach^{27,28} treats specified nuclei, typically protons, as well as all electrons quantum mechanically, thereby offering an alternative strategy. Many analogues of conventional electronic structure methods have been implemented within the NEO framework, including density functional theory,^{29–31} time-dependent density functional theory (TDDFT),^{32,33} coupled-cluster theory,^{34–36} density matrix renormalization group,^{37,38} and the complete active space self-consistent field method.^{27,39}

To capture the bilobal nature of the hydrogen nuclear wavefunction in tunneling systems within the NEO framework, a multireference method is required.^{40–46} Typically, the transferring hydrogen nucleus is represented by two basis function centers, each with a protonic and an electronic basis set.^{40–46} The NEO nonorthogonal configuration interaction (NEO-NOCI) method has been used to obtain tunneling splittings of simple systems,⁴³ but the formalism would need to be extended significantly to be more generally applicable. The NEO multistate density functional theory (NEO-MSDFT) method has been used to study larger tunneling systems, in some cases with multiple tunneling protons.^{44,45} The NEO-MSDFT method depends on tunable parameters and approximate functionals to obtain quantitatively accurate tunneling splittings, but it is useful for real-time nuclear-electronic quantum dynamics simulations in large chemical and biological systems.^{47,48} A more rigorous wavefunction-based method that is systematically improvable and can provide accurate tunneling splittings for molecular systems without free parameters is desirable.

In this Letter, we apply the recently introduced NEO-MRCI method⁴⁹ to several hydrogen tunneling systems, demonstrating it can be used to calculate accurate tunneling splittings for fixed geometries. Analogous to the conventional MRCI method,^{50,51} the NEO-MRCI method is parameter-free and offers a natural description of excited states, which are vibronic states within the NEO framework. As a multireference method, it is well-suited to tunneling problems within the NEO framework. In contrast to most other methods for computing tunneling splittings, the electronic

and nuclear wavefunctions are computed simultaneously with no Born-Oppenheimer separation between the electrons and the transferring proton. The four hydrogen tunneling systems studied in this work are HeHHe^+ , OCHCO^+ , FHF^- , and malonaldehyde. The HeHHe^+ , OCHCO^+ , and FHF^- systems exhibit hydrogen tunneling at extended donor-acceptor distances.⁵² Malonaldehyde is a prototypical system for studying intramolecular hydrogen tunneling and has been studied widely both experimentally and theoretically.^{9,24,25,53–57}

To benchmark the NEO-MRCI results, the three-dimensional Fourier Grid Hamiltonian (FGH)^{58,59} method was used to compute numerically exact reference tunneling splittings. The FGH method solves for the proton vibrational wavefunctions given a three-dimensional electronic potential energy surface generated by moving the transferring hydrogen nucleus on a grid while the other nuclei remain fixed. In this work, the energy at each grid point was computed with the conventional electronic coupled-cluster singles and doubles (CCSD) method. The aug-cc-pVTZ⁶⁰ electronic basis set was used for HeHHe^+ , OCHCO^+ , and FHF^- , and the cc-pVTZ⁶¹ electronic basis set was used for malonaldehyde. The resulting proton vibrational wavefunctions and tunneling splittings are directly comparable to NEO calculations for fixed geometries of the classical nuclei. Note that the tunneling splittings computed for fixed geometries are not comparable to experimentally measured tunneling splittings because the hydrogen tunneling mode is typically coupled to the vibrational modes of other nuclei. The effect of this coupling can be included using a method such as vibronic coupling theory.⁶² To benchmark the NEO-MRCI method for electronically adiabatic hydrogen tunneling splittings, however, the FGH results provide a numerically exact reference.

The NEO-MRCI wavefunction is an expansion of NEO configurations:

$$\Psi^{\text{NEO}}(\mathbf{R}^c) = \sum_{\mu} c_{\mu}(\mathbf{R}^c) \psi_{\mu}^{\text{NEO}}(\mathbf{R}^c) \quad (1)$$

where each configuration ψ_{μ}^{NEO} is the product of electronic and protonic Slater determinants

$$\psi_{\mu}^{\text{NEO}}(\mathbf{R}^c) = |\Phi_{i(\mu)}^e(\mathbf{R}^c)\rangle |\Phi_{I(\mu)}^p(\mathbf{R}^c)\rangle. \quad (2)$$

Here \mathbf{R}^c are the coordinates of the classically treated nuclei and are fixed during the NEO-MRCI calculation. $|\Phi_{i(\mu)}^e\rangle$ and $|\Phi_{I(\mu)}^p\rangle$ are the i -th electronic determinant and I -th protonic determinant, respectively, that form the μ -th NEO configuration, ψ_{μ}^{NEO} . The electronic and protonic determinants are composed of electronic and protonic orbitals optimized in the NEO-MCSCF reference space defined by electronic and protonic active spaces.⁴⁹ In this work, the orbitals are optimized for the lowest two vibronic states using the state averaged NEO-MCSCF (NEO-SA-MCSCF) method. The NEO-MR-SD_{en}CI expansion is constructed from single electron, single proton, and double electron-proton excitations from this reference space.⁴⁹

We calculated hydrogen tunneling splittings for HeHHe⁺, FHF⁻, and OCHCO⁺ at various He—He, F—F, and C—C distances and at two geometries of malonaldehyde. The geometry used for OCHCO⁺ was obtained from earlier work,⁴⁴ and the C—O distances for each CO moiety were kept fixed as the C—C distance was increased. For malonaldehyde, an average of reactant and product structures was used, where the reactant and product correspond to the hydrogen optimized near the donor or acceptor, respectively. We examined two malonaldehyde geometries, where one structure was generated using the equilibrium reactant and product geometries, corresponding to an O—O distance of 2.617 Å, rounded to 2.62 Å in the rest of the paper, and the other structure was generated with the O—O distance constrained to 2.55 Å during optimization of the reactant and product structures. These geometry optimizations were performed at the conventional CCSD/cc-pVTZ level of theory, and the coordinates are given in Section 6.4 of the SI.

In all NEO calculations, the hydrogen basis function center positions were optimized with conventional CCSD. For each geometry, the proton was optimized near the donor atom with all other nuclei held fixed. One proton basis function center was placed at the optimized position, and the other was placed at the mirror image near the acceptor for symmetric systems. For non-symmetric systems, the position of the second proton basis function center would be determined by a second optimization near the acceptor. This procedure results in proton basis function centers positioned at the minima of the electronically adiabatic CCSD double-well potential energy surface. As shown from the examples below, optimizing the basis function center positions at the conventional CCSD

level provides a reliable method for computing hydrogen tunneling splittings with the NEO-MRCI method.

Accurate tunneling splittings require large electronic and protonic basis sets, in accordance with previous work demonstrating that accurate vibronic excitation energies computed with NEO-TDDFT require large electronic basis sets.³³ The HeHHe⁺ and FHF⁻ NEO calculations used the even-tempered 8s8p8d8f³⁰ protonic basis set. To reduce computational cost, the OCHCO⁺ and malonaldehyde NEO calculations used an even-tempered 5s5p5d5f protonic basis set, where $\alpha = 2.8$ and $\beta = 1.8459$ according to the standard formula,⁶³ covering the same exponent range as 8s8p8d8f. We show that the same tunneling splitting is obtained for HeHHe⁺ using the 8s8p8d8f and 5s5p5d5f basis sets (Table S5). All NEO calculations used the cc-pV5Z* electronic basis set for the quantum proton. The asterisk indicates that the most diffuse basis function from the core contraction is used to represent the 1s orbital, while the rest of the primitives from the core contraction are removed. Previous work has shown that NEO calculations should not use the same electronic basis sets as conventional calculations because the quantized proton is no longer a point charge.⁴⁹ Results with different protonic and electronic basis sets are provided in the SI to show convergence (Tables S1-S6). The remaining atoms in the NEO calculations were represented with the same electronic basis set used in the corresponding FGH calculation: aug-cc-pVTZ for HeHHe⁺, FHF⁻, and OCHCO⁺, and cc-pVTZ for malonaldehyde. These same electronic basis sets were used for all atoms in the conventional CCSD proton basis function center optimizations.

The molecular orbitals were optimized in a NEO-SA-MCSCF calculation, weighing the two lowest vibronic states equally. To ensure the electronic and protonic molecular orbitals are symmetric, the initial guess orbitals were generated from a two-proton NEO-HF calculation. Although this molecule containing an additional proton is unphysical, the resulting orbitals serve as a reasonable initial guess for the NEO-SA-MCSCF calculation. Full protonic active spaces were used for all systems in this work. A minimal (2e, 2o) active space, containing orbitals of in-phase σ and σ^* character, was used for FHF⁻, OCHCO⁺, and malonaldehyde (Figures S2-S4). It is interesting to note that the same (2e, 2o) active space was used to predict accurate tunneling splittings

in three different systems. HeHHe^+ is different from the other systems in that it resembles a bare proton transferring between the donor and acceptor with negligible electron density in the central region of the molecule (Fig. S1). Because the chemical bonding structure is qualitatively different for HeHHe^+ in that the covalent sigma bond between helium and hydrogen is not formed, a single-reference electronic treatment within NEO-CASSCF is sufficient for this system. The NEO calculations to obtain deuterium tunneling splittings for FDF^- and malonaldehyde were performed with the same active spaces and basis sets as the hydrogen calculations.

The hydrogen tunneling splittings calculated for HeHHe^+ at the NEO-MR- $\text{SD}_{\text{en}}\text{CI}$ level agree quantitatively with the tunneling splittings calculated using the numerically exact FGH method. As expected, the tunneling splitting decreases with increased He—He distance due to the increasing barrier height and width (Fig. 2a). The NEO-MR- $\text{SD}_{\text{en}}\text{CI}$ protonic densities also exhibit the correct qualitative behavior (Fig. 3). The ground and first excited state protonic densities are bilobal, and the ground state proton vibrational density has no nodes, whereas the first excited state proton density contains a single node. The other two linear systems behave similarly to HeHHe^+ despite having more complex electronic structures. The NEO-MR- $\text{SD}_{\text{en}}\text{CI}$ tunneling splittings of FHF^- and OCHCO^+ decrease as the donor-acceptor distance increases and quantitatively agree with the FGH tunneling splittings (Fig. 2b and c).

The malonaldehyde results further demonstrate the broad applicability of the NEO-MRCI method to tunneling problems. The tunneling splittings for the two malonaldehyde geometries corresponding to different O—O distances are shown in Figure 4a. NEO-MR- $\text{SD}_{\text{en}}\text{CI}$ tunneling splittings for both of these geometries are in excellent agreement with the FGH benchmarks. The protonic densities are bilobal with the appropriate nodal structure but are slightly squeezed to form a "V" shape (Fig. 4c). This behavior is consistent with previous studies demonstrating that malonaldehyde follows a non-linear tunneling path.^{54,55} This level of agreement in the tunneling splittings for a larger, non-linear molecule supports the application of NEO-MR- $\text{SD}_{\text{en}}\text{CI}$ for studying other interesting hydrogen tunneling systems.

The NEO-MR- $\text{SD}_{\text{en}}\text{CI}$ method can also be used to calculate deuterium tunneling splittings.

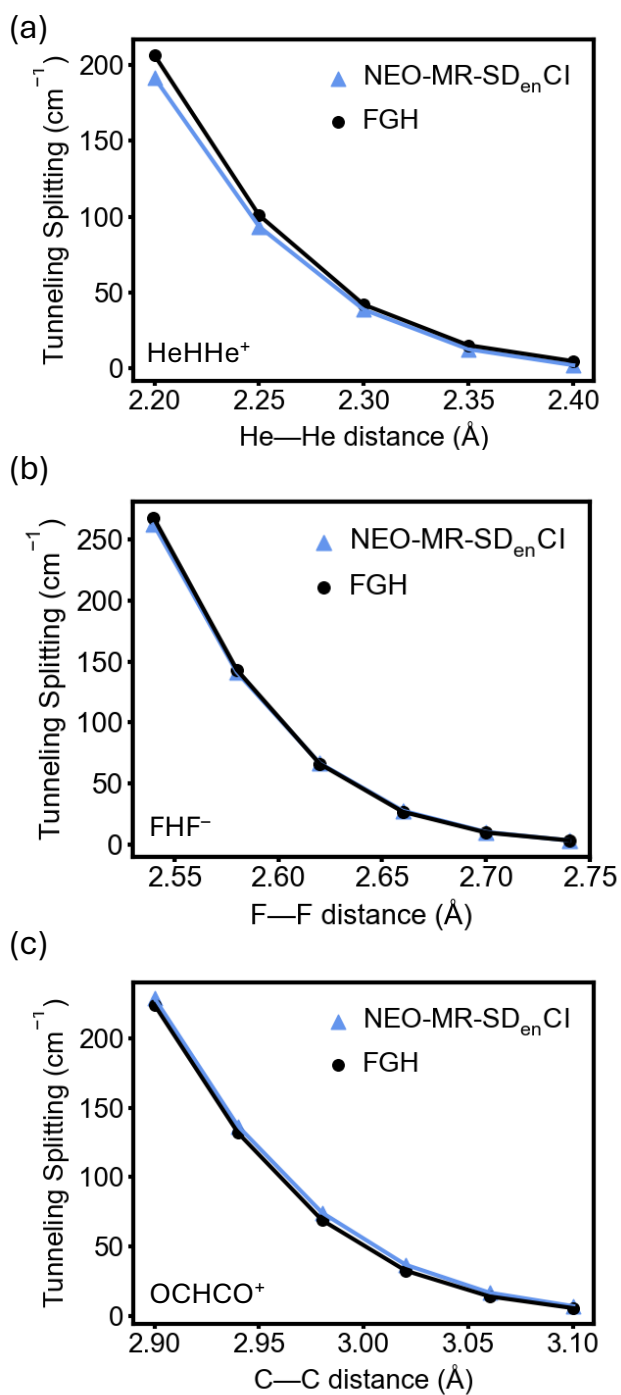


Figure 2. NEO-MR-SD_{en}CI hydrogen tunneling splittings compared with the reference FGH results for (a) HeHHe⁺, (b) FHF⁻, and (c) OCHCO⁺ at different donor-acceptor distances. The reference FGH results were computed at the conventional CCSD/aug-cc-pVTZ level of theory. The numerical values are provided in Tables S1-S3.

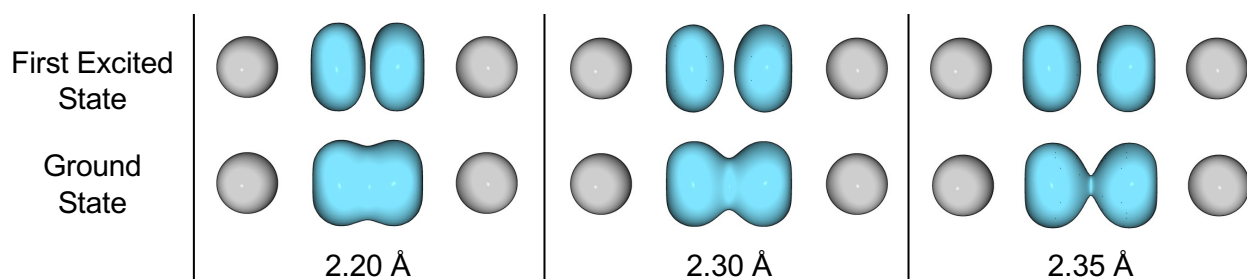


Figure 3. NEO-MR-SD_{en}CI protonic densities for HeHHe⁺ at the indicated He—He distances. The He atoms are shown in light gray, and the protonic densities are shown in cyan with an isovalue of 0.04 e Bohr⁻³. The analogous protonic densities for the other systems are shown in Figures S5 and S6.

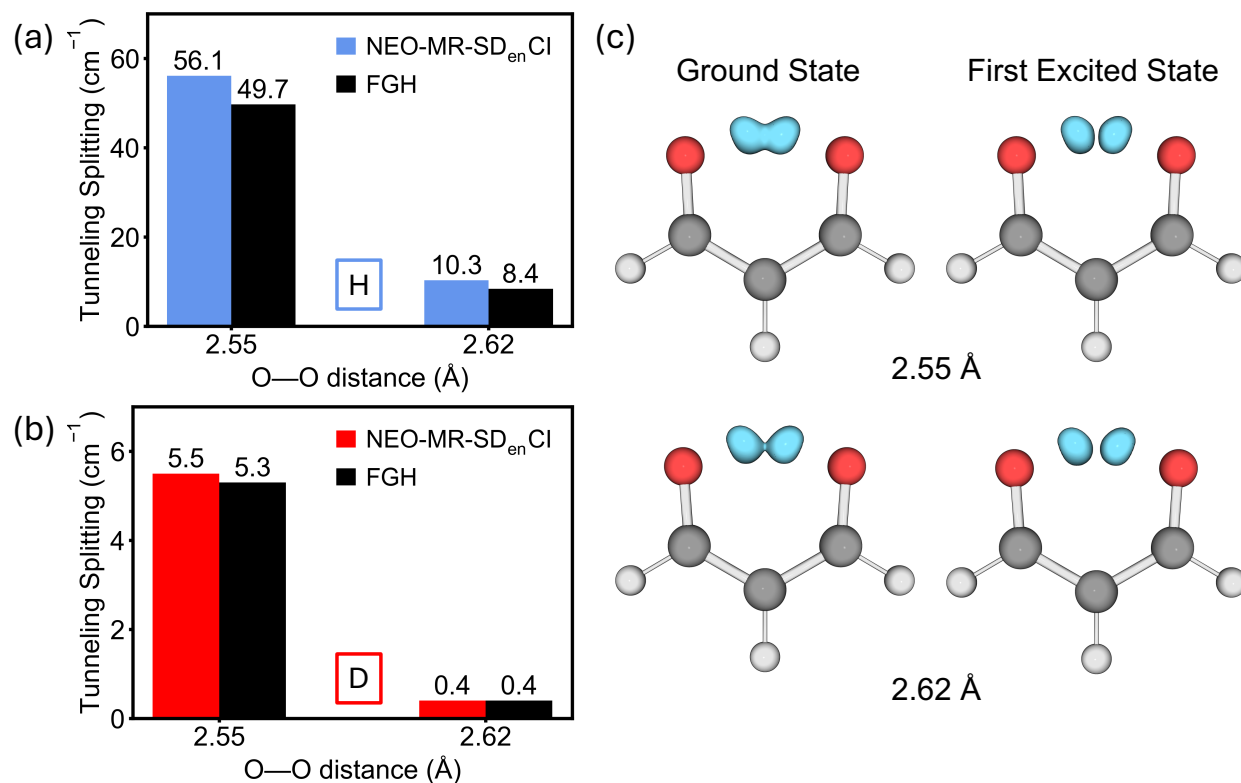


Figure 4. NEO-MR-SD_{en}CI tunneling splittings for malonaldehyde at two different donor-acceptor distances compared to the FGH results with (a) hydrogen and (b) deuterium. The FGH results were computed at the CCSD/cc-pVTZ level of theory. (c) Protonic densities for hydrogen at the indicated O—O distances. The protonic densities are shown in cyan with an isovalue of 0.04 e Bohr⁻³, and the other atoms are shown in dark gray (carbon), red (oxygen), and light gray (hydrogen).

We calculated the deuterium tunneling splittings for the FDF^- and malonaldehyde systems. As shown in Figure 5, the NEO-MR- $\text{SD}_{\text{en}}\text{CI}$ deuterium tunneling splittings are in excellent agreement with the FGH results at a range of donor-acceptor distances for FDF^- . The deuterium tunneling splittings are much smaller than the hydrogen tunneling splittings, as expected for a heavier quantum nucleus. The NEO-MR- $\text{SD}_{\text{en}}\text{CI}$ deuterium tunneling splittings for malonaldehyde also agree well with the FGH reference results and follow the same trend as the FDF^- deuterium tunneling splittings (Fig. 4b).

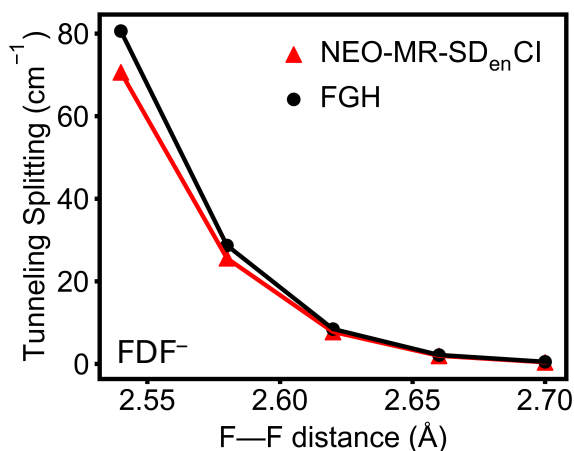


Figure 5. NEO-MR- $\text{SD}_{\text{en}}\text{CI}$ deuterium tunneling splittings compared with the reference FGH results for FDF^- at different donor-acceptor distances. The reference FGH results were computed at the conventional CCSD/aug-cc-pVTZ level of theory. The numerical values are provided in Table S2.

Hydrogen tunneling systems are a challenge to model due to their multireference nature in the NEO framework and the small magnitudes of typical tunneling splittings. In this Letter, we have demonstrated that NEO-MRCI is an effective method for calculating tunneling splittings for molecular systems. NEO-MRCI does not require any parameters, accounts for the multireference nature of the system, and captures the correlation energy required to obtain quantitatively accurate results. Moreover, the NEO-MRCI method can describe hydrogen tunneling in systems with both linear and non-linear tunneling paths, such as malonaldehyde. We have devised an efficient and unbiased strategy using conventional CCSD optimizations to determine the proton basis function center positions. We demonstrate that relatively large electronic and protonic basis sets, as well as a

(2e, 2o) active space consisting of in-phase σ and σ^* orbitals, can effectively describe the vibronic tunneling states in a variety of systems. With these insights, the NEO-MRCI approach produces accurate hydrogen tunneling splittings in applications to four different molecular systems at a range of donor-acceptor distances. Additionally, this scheme produces accurate deuterium tunneling splittings. These results show that the NEO-MRCI approach is promising for investigating a wide range of hydrogen tunneling systems in chemistry and biology.

Acknowledgement

The authors thank Dr. Scott Garner, Dr. Jonathan Fetherolf, Dr. Eno Paenurk, Dr. Chiara Aieta, Joseph Dickinson, Mathew Chow, Millan Welman, and Rowan Goudy for useful discussions. This work was supported by the National Science Foundation Grant No. CHE-2408934.

Supporting Information Available

The Supporting Information is available free of charge. Tunneling splitting data, basis set convergence data, electron density, electronic active spaces, OCHCO⁺ and FHF⁻ protonic densities, molecular coordinates.

References

- (1) Cha, Y.; Murray, C. J.; Klinman, J. P. Hydrogen Tunneling in Enzyme Reactions. *Science* **1989**, *243*, 1325–1330.
- (2) Hoganson, C. W.; Babcock, G. T. A Metalloradical Mechanism for the Generation of Oxygen from Water in Photosynthesis. *Science* **1997**, *277*, 1953–1956.
- (3) Knapp, M. J.; Rickert, K.; Klinman, J. P. Temperature-Dependent Isotope Effects in Soybean

- Lipoxygenase-1: Correlating Hydrogen Tunneling with Protein Dynamics. *J. Am. Chem. Soc.* **2002**, *124*, 3865–3874.
- (4) Stubbe, J.; Nocera, D. G.; Yee, C. S.; Chang, M. C. Y. Radical Initiation in the Class I Ribonucleotide Reductase: Long-Range Proton-Coupled Electron Transfer? *Chem. Rev.* **2003**, *103*, 2167–2202.
- (5) Magnuson, A.; Anderlund, M.; Johansson, O.; Lindblad, P.; Lomoth, R.; Polivka, T.; Ott, S.; Stensjö, K.; Styring, S.; Sundström, V. et al. Biomimetic and Microbial Approaches to Solar Fuel Generation. *Acc. Chem. Res.* **2009**, *42*, 1899–1909.
- (6) Hammes-Schiffer, S.; Stuchebrukhov, A. A. Theory of Coupled Electron and Proton Transfer Reactions. *Chem. Rev.* **2010**, *110*, 6939–6960.
- (7) Warren, J. J.; Tronic, T. A.; Mayer, J. M. Thermochemistry of Proton-Coupled Electron Transfer Reagents and its Implications. *Chem. Rev.* **2010**, *110*, 6961–7001.
- (8) DuBois, D. L.; Bullock, R. M. Molecular Electrocatalysts for the Oxidation of Hydrogen and the Production of Hydrogen – The Role of Pendant Amines as Proton Relays. *Eur. J. Inorg. Chem.* **2011**, *2011*, 1017–1027.
- (9) Firth, D. W.; Beyer, K.; Dvorak, M. A.; Reeve, S. W.; Grushow, A.; Leopold, K. R. Tunable far-infrared spectroscopy of malonaldehyde. *J. Chem. Phys.* **1991**, *94*, 1812–1819.
- (10) Birer, Ö.; Havenith, M. High-Resolution Infrared Spectroscopy of the Formic Acid Dimer. *Annu. Rev. Phys. Chem.* **2009**, *60*, 263–275.
- (11) Vdovin, A.; Waluk, J.; Dick, B.; Slenczka, A. Mode-Selective Promotion and Isotope Effects of Concerted Double-Hydrogen Tunneling in Porphycene Embedded in Superfluid Helium Nanodroplets. *ChemPhysChem* **2009**, *10*, 761–765.
- (12) Talbot, J. J.; Yang, N.; Huang, M.; Duong, C. H.; McCoy, A. B.; Steele, R. P.; Johnson, M. A.

- Spectroscopic Signatures of Mode-Dependent Tunnel Splitting in the Iodide–Water Binary Complex. *J. Phys. Chem. A*. **2020**, *124*, 2991–3001.
- (13) Sen, A.; Kohen, A. Enzymatic tunneling and kinetic isotope effects: chemistry at the crossroads. *J. Phys. Org. Chem.* **2010**, *23*, 613–619.
- (14) Hama, T.; Ueta, H.; Kouchi, A.; Watanabe, N. Quantum tunneling observed without its characteristic large kinetic isotope effects. *Proc. Natl. Acad. Sci. U.S.A.* **2015**, *112*, 7438–7443.
- (15) Klinman, J. P.; Offenbacher, A. R. Understanding Biological Hydrogen Transfer Through the Lens of Temperature Dependent Kinetic Isotope Effects. *Acc. Chem. Res.* **2018**, *51*, 1966–1974.
- (16) Hammes-Schiffer, S. Explaining Kinetic Isotope Effects in Proton-Coupled Electron Transfer Reactions. *Acc. Chem. Res.* **2025**, *58*, 1335–1344.
- (17) Mil'nikov, G. V.; Nakamura, H. Practical implementation of the instanton theory for the ground-state tunneling splitting. *J. Chem. Phys.* **2001**, *115*, 6881–6897.
- (18) Richardson, J. O.; Althorpe, S. C. Ring-polymer instanton method for calculating tunneling splittings. *J. Chem. Phys.* **2011**, *134*, 054109.
- (19) Trenins, G.; Meuser, L.; Bertschi, H.; Vavourakis, O.; Flütsch, R.; Richardson, J. O. Exact tunneling splittings from symmetrized path integrals. *J. Chem. Phys.* **2023**, *159*.
- (20) Gregory, J. K.; Clary, D. C. Calculations of the tunneling splittings in water dimer and trimer using diffusion Monte Carlo. *J. Chem. Phys.* **1995**, *102*, 7817–7829.
- (21) Fortenberry, R. C.; Yu, Q.; Mancini, J. S.; Bowman, J. M.; Lee, T. J.; Crawford, T. D.; Klemperer, W. F.; Francisco, J. S. Communication: Spectroscopic consequences of proton delocalization in OCHCO⁺. *J. Chem. Phys.* **2015**, *143*, 071102.

- (22) DiRisio, R. J.; Finney, J. M.; McCoy, A. B. Diffusion Monte Carlo approaches for studying nuclear quantum effects in fluxional molecules. *Wiley Interdiscip. Rev. Comput. Mol. Sci.* **2022**, *12*, e1615.
- (23) Finney, J. M.; McCoy, A. B. Correlations between the Structures and Spectra of Protonated Water Clusters. *J. Phys. Chem. A* **2024**, *128*, 868–879.
- (24) Coutinho-Neto, M. D.; Viel, A.; Manthe, U. The ground state tunneling splitting of malonaldehyde: Accurate full dimensional quantum dynamics calculations. *J. Chem. Phys.* **2004**, *121*, 9207–9210.
- (25) Schröder, M.; Gatti, F.; Meyer, H.-D. Theoretical studies of the tunneling splitting of malonaldehyde using the multiconfiguration time-dependent Hartree approach. *J. Chem. Phys.* **2011**, *134*, 234307.
- (26) Suzuki, K.; Kanno, M.; Koseki, S.; Kono, H. A Structure-Based Gaussian Expansion for Quantum Reaction Dynamics in Molecules: Application to Hydrogen Tunneling in Malonaldehyde. *J. Phys. Chem. A* **2023**, *127*, 4152–4165.
- (27) Webb, S. P.; Iordanov, T.; Hammes-Schiffer, S. Multiconfigurational nuclear-electronic orbital approach: Incorporation of nuclear quantum effects in electronic structure calculations. *J. Chem. Phys.* **2002**, *117*, 4106–4118.
- (28) Hammes-Schiffer, S. Nuclear–electronic orbital methods: Foundations and prospects. *J. Chem. Phys.* **2021**, *155*, 030901.
- (29) Pak, M. V.; Chakraborty, A.; Hammes-Schiffer, S. Density Functional Theory Treatment of Electron Correlation in the Nuclear-Electronic Orbital Approach. *J. Phys. Chem. A* **2007**, *111*, 4522–4526.
- (30) Yang, Y.; Brorsen, K. R.; Culpitt, T.; Pak, M. V.; Hammes-Schiffer, S. Development of a prac-

- tical multicomponent density functional for electron-proton correlation to produce accurate proton densities. *J. Chem. Phys.* **2017**, *147*, 114113.
- (31) Brorsen, K. R.; Yang, Y.; Hammes-Schiffer, S. Multicomponent Density Functional Theory: Impact of Nuclear Quantum Effects on Proton Affinities and Geometries. *J. Phys. Chem. Lett.* **2017**, *8*, 3488–3493.
- (32) Yang, Y.; Culpitt, T.; Hammes-Schiffer, S. Multicomponent Time-Dependent Density Functional Theory: Proton and Electron Excitation Energies. *J. Phys. Chem. Lett.* **2018**, *9*, 1765–1770.
- (33) Culpitt, T.; Yang, Y.; Pavošević, F.; Tao, Z.; Hammes-Schiffer, S. Enhancing the applicability of multicomponent time-dependent density functional theory. *J. Chem. Phys.* **2019**, *150*, 201101.
- (34) Pavošević, F.; Culpitt, T.; Hammes-Schiffer, S. Multicomponent Coupled Cluster Singles and Doubles Theory within the Nuclear-Electronic Orbital Framework. *J. of Chem. Theory Comput.* **2019**, *15*, 338–347.
- (35) Pavošević, F.; Tao, Z.; Hammes-Schiffer, S. Multicomponent Coupled Cluster Singles and Doubles with Density Fitting: Protonated Water Tetramers with Quantized Protons. *J. Chem. Phys. Lett.* **2021**, *12*, 1631–1637.
- (36) Pavošević, F.; Hammes-Schiffer, S. Triple electron–electron–proton excitations and second-order approximations in nuclear–electronic orbital coupled cluster methods. *J. of Chem. Phys.* **2022**, *157*, 074104.
- (37) Muolo, A.; Baiardi, A.; Feldmann, R.; Reiher, M. Nuclear-electronic all-particle density matrix renormalization group. *The Journal of Chemical Physics* **2020**, *152*, 204103.
- (38) Feldmann, R.; Muolo, A.; Baiardi, A.; Reiher, M. Quantum Proton Effects from Density Matrix Renormalization Group Calculations. *J. Chem. Theory Comput.* **2022**, *18*, 234–250.

- (39) Fajen, O. J.; Brorsen, K. R. Multicomponent CASSCF Revisited: Large Active Spaces Are Needed for Qualitatively Accurate Protonic Densities. *J. Chem. Theory Comput.* **2021**, *17*, 965–974.
- (40) Pak, M. V.; Hammes-Schiffer, S. Electron-Proton Correlation for Hydrogen Tunneling Systems. *Phys. Rev. Lett.* **2004**, *92*, 103002.
- (41) Pak, M. V.; Swalina, C.; Webb, S. P.; Hammes-Schiffer, S. Application of the nuclear–electronic orbital method to hydrogen transfer systems: multiple centers and multi-configurational wavefunctions. *Chem. Phys.* **2004**, *304*, 227–236.
- (42) Swalina, C.; Pak, M. V.; Hammes-Schiffer, S. Analysis of the nuclear-electronic orbital method for model hydrogen transfer systems. *J. Chem. Phys.* **2005**, *123*.
- (43) Skone, J. H.; Pak, M. V.; Hammes-Schiffer, S. Nuclear-electronic orbital nonorthogonal configuration interaction approach. *J. Chem. Phys.* **2005**, *123*, 134108.
- (44) Yu, Q.; Hammes-Schiffer, S. Nuclear-Electronic Orbital Multistate Density Functional Theory. *J. Phys. Chem. Lett* **2020**, *11*, 10106–10113.
- (45) Dickinson, J. A.; Yu, Q.; Hammes-Schiffer, S. Generalized Nuclear-Electronic Orbital Multistate Density Functional Theory for Multiple Proton Transfer Processes. *J. Phys. Chem. Lett* **2023**, *14*, 6170–6178.
- (46) Garner, S. M.; Upadhyay, S.; Li, X.; Hammes-Schiffer, S. Nuclear–Electronic Orbital Time-Dependent Configuration Interaction Method. *J. Phys. Chem. Lett* **2024**, *15*, 6017–6023.
- (47) Yu, Q.; Roy, S.; Hammes-Schiffer, S. Nonadiabatic Dynamics of Hydrogen Tunneling with Nuclear-Electronic Orbital Multistate Density Functional Theory. *J. Chem. Theory Comput.* **2022**, *18*, 7132–7141.

- (48) Dickinson, J. A.; Hammes-Schiffer, S. Nonadiabatic Hydrogen Tunneling Dynamics for Multiple Proton Transfer Processes with Generalized Nuclear-Electronic Orbital Multistate Density Functional Theory. *J. Chem. Theory Comput.* **2024**, *20*, 7716–7727.
- (49) Malbon, C.; Hammes-Schiffer, S. Nuclear-Electronic Orbital Multireference Configuration Interaction for Ground and Excited Vibronic States and Fundamental Insights into Multi-component Basis Sets. *J. Chem. Theory Comput.* **2025**,
- (50) Lischka, H.; Nachtigallová, D.; Aquino, A. J. A.; Szalay, P. G.; Plasser, F.; Machado, F. B. C.; Barbatti, M. Multireference Approaches for Excited States of Molecules. *Chem. Rev.* **2018**, *118*, 7293–7361.
- (51) Matsika, S. Electronic Structure Methods for the Description of Nonadiabatic Effects and Conical Intersections. *Chem. Rev.* **2021**, *121*, 9407–9449.
- (52) Terrill, K.; Nesbitt, D. J. Ab initio anharmonic vibrational frequency predictions for linear proton-bound complexes OC–H+–CO and N₂–H+–N₂. *Phys. Chem. Chem. Phys.* **2010**, *12*, 8311–8322.
- (53) Baughcum, S. L.; Smith, Z.; Wilson, E. B.; Duerst, R. W. Microwave spectroscopic study of malonaldehyde. 3. Vibration-rotation interaction and one-dimensional model for proton tunneling. *J. Am. Chem. Soc.* **1984**, *106*, 2260–2265.
- (54) Shida, N.; Barbara, P. F.; Almlöf, J. E. A theoretical study of multidimensional nuclear tunneling in malonaldehyde. *J. Chem. Phys.* **1989**, *91*, 4061–4072.
- (55) Tautermann, C. S.; Voegelé, A. F.; Loerting, T.; Liedl, K. R. The optimal tunneling path for the proton transfer in malonaldehyde. *J. Chem. Phys.* **2002**, *117*, 1962–1966.
- (56) Vaillant, C. L.; Wales, D. J.; Althorpe, S. C. Tunneling splittings from path-integral molecular dynamics using a Langevin thermostat. *The Journal of Chemical Physics* **2018**, *148*, 234102.

- (57) Baumann, J.; Trenins, G.; and, J. O. R. The exact tunnelling splitting of malonaldehyde from symmetrized path-integral molecular dynamics. *Mol. Phys.* **2025**, *0*, e2474202.
- (58) Marston, C. C.; Balint-Kurti, G. G. The Fourier grid Hamiltonian method for bound state eigenvalues and eigenfunctions. *J. Chem. Phys.* **1989**, *91*, 3571–3576.
- (59) Webb, S. P.; Hammes-Schiffer, S. Fourier grid Hamiltonian multiconfigurational self-consistent-field: A method to calculate multidimensional hydrogen vibrational wavefunctions. *J. Chem. Phys.* **2000**, *113*, 5214–5227.
- (60) Kendall, R. A.; Dunning, J., Thom H.; Harrison, R. J. Electron affinities of the first-row atoms revisited. Systematic basis sets and wave functions. *J. Chem. Phys.* **1992**, *96*, 6796–6806.
- (61) Dunning, J., Thom H. Gaussian basis sets for use in correlated molecular calculations. I. The atoms boron through neon and hydrogen. *J. Chem. Phys.* **1989**, *90*, 1007–1023.
- (62) Hazra, A.; Skone, J. H.; Hammes-Schiffer, S. Combining the nuclear-electronic orbital approach with vibronic coupling theory: Calculation of the tunneling splitting for malonaldehyde. *J. Chem. Phys.* **2009**, *130*.
- (63) Helgaker, T.; Jørgensen, P.; Olsen, J. *Molecular Electronic-Structure Theory*; John Wiley & Sons, Ltd, 2000; Chapter 8, pp 287–335.

Supporting Information

Computing Hydrogen Tunneling Splittings with Nuclear-Electronic Orbital Multireference Configuration Interaction

Rachel J. Stein, Christopher L. Malbon, and Sharon Hammes-Schiffer*

Department of Chemistry, Princeton University, Princeton, NJ 08544

E-mail: shs566@princeton.edu

Contents

1	Tunneling Splitting Tables	S3
2	Basis Set Convergence	S5
3	Electron Density	S6
4	Electronic Active Spaces	S7
5	OCHCO⁺ and FHF⁻ Protonic Densities	S8
6	Coordinates	S9
6.1	HeHHe ⁺	S9
6.2	FHF ⁻	S10
6.3	OCHCO ⁺	S11
6.4	Malondaldehyde	S13

1 Tunneling Splitting Tables

Table S1. HeHHe⁺ Tunneling Splittings (in cm⁻¹) with Hydrogen and Deuterium Computed with NEO-MR-SD_{en}CI Compared to FGH Benchmark

He—He (Å)	NEO-MR-SD _{en} CI ^a			FGH ^b	
	H (8s8p8d)	H (8s8p8d8f)	D (8s8p8d8f)	H	D
2.20	227.8	191.6	48.3	206.5	64.1
2.25	118.8	93.5	14.0	101.0	20.4
2.30	55.1	38.8	2.4	42.1	5.3
2.35	23.2	12.8	0.6	15.4	1.2
2.40 ^c	9.0	2.3	NA	4.9	NA

^a The basis function center positions are optimized at the CCSD/aug-cc-pVTZ level of theory. The indicated protonic basis set and the cc-pV5Z* electronic basis set are used on the proton basis function centers. The aug-cc-pVTZ electronic basis set is used on He. No electronic active space and a full protonic active space are used.

^b The FGH results were computed at the CCSD/aug-cc-pVTZ level of theory. The grid is 32×32×32 with a step size of 0.055 Å. The grid ranges from -0.820 to 0.875 Å in the *x*, *y*, and *z* directions with the molecule centered at the origin.

^c The deuterium splitting is too small to calculate reliably with these methods at this distance.

Table S2. FHF⁻ Tunneling Splittings (in cm⁻¹) with Hydrogen and Deuterium Computed with NEO-MR-SD_{en}CI Compared to FGH Benchmark

F—F (Å)	NEO-MR-SD _{en} CI ^a			FGH ^b	
	H (8s8p8d)	H (8s8p8d8f)	D (8s8p8d8f)	H	D
2.54	248.4	262.5	70.6	267.9	80.6
2.58	127.3	141.3	25.6	143.3	28.7
2.62	57.9	66.4	7.7	66.0	8.4
2.66	23.8	27.5	1.9	26.7	2.1
2.70	6.2	10.1	0.4	9.7	0.5
2.74 ^c	3.1	3.1	NA	3.2	NA

^a The basis function center positions are optimized at the CCSD/aug-cc-pVTZ level of theory. The indicated protonic basis set and the cc-pV5Z* electronic basis set are used on the proton basis function centers. The aug-cc-pVTZ electronic basis set is used on F. A (2e, 2o) electronic active space and a full protonic active space are used.

^b The FGH results were computed at the CCSD/aug-cc-pVTZ level of theory. The grid is 32×32×32 with a step size of 0.074 Å. The grid ranges from -1.113 to 1.187 Å in the *x*, *y*, and *z* directions with the molecule centered at the origin.

^c The deuterium splitting is too small to calculate reliably with these methods at this distance.

Table S3. OCHCO⁺ Tunneling Splittings (in cm⁻¹) Computed with NEO-MR-SD_{en}CI Compared to FGH Benchmark

C—C(Å)	NEO-MR-SD _{en} CI ^a		FGH ^b
	8s8p8d	5s5p5d5f	
2.90	196.4	229.2	224.3
2.94	106.8	136.7	131.8
2.98	53.8	74.5	69.1
3.02	24.6	36.9	32.6
3.06	10.3	16.8	14.1
3.10	3.9	7.1	5.6

^a The basis function center positions are optimized at the CCSD/aug-cc-pVTZ level of theory. The indicated protonic basis set and the cc-pV5Z* electronic basis set are used on the proton basis function centers. The aug-cc-pVTZ electronic basis set is used on O and C. A (2e, 2o) electronic active space and a full protonic active space are used.

^b The FGH results were computed at the CCSD/aug-cc-pVTZ level of theory. The grid is 32×32×32 with a step size of 0.06 Å. The grid ranges from -0.93 to 0.93 Å in the *x*, *y*, and *z* directions with the molecule centered at the origin.

Table S4. Malonaldehyde Tunneling Splittings (in cm⁻¹) Computed with NEO-MR-SD_{en}CI Compared to FGH Benchmark

O—O(Å)	NEO-MR-SD _{en} CI ^a			FGH ^b	
	H (8s8p8d)	H (5s5p5d5f)	D (5s5p5d5f)	H	D
2.55	36.0	56.1	5.5	49.7	5.3
2.62	5.4	10.3	0.4	8.4	0.4

^a The basis function center positions are optimized at the CCSD/aug-cc-pVTZ level of theory. The indicated protonic basis set and the cc-pV5Z* electronic basis set are used on the proton basis function centers. The aug-cc-pVTZ electronic basis set is used on the other atoms. A (2e, 2o) electronic active space and a full protonic active space are used.

^b The FGH results were computed at the CCSD/cc-pVTZ level of theory. The grid is 32×32×32 with a step size of 0.06 Å and ranges from -0.93 to 0.93 Å in the *x* and *z* directions for both geometries, as well as from -1.253 to 0.607 Å (from -1.271 to 0.589 Å) in the *y* direction for the O—O distance of 2.55 Å (2.62 Å) with the malonaldehyde coordinates given in Section 6.4.

2 Basis Set Convergence

Table S5. HeHHe⁺ Tunneling Splittings (in cm⁻¹) Computed with NEO-MR-SD_{en}CI with Varying Protonic and Electronic Basis Sets^a

Protonic Basis Set	Electronic Basis Set	NEO-MR-SD _{en} CI ^b
8s8p8d	cc-pV5Z*	55.1
8s8p8d8f	cc-pV5Z*	38.8
5s5p5d5f5g	cc-pV5Z*	35.4
8s8p8d8f	cc-pVQZ*	45.6
8s8p8d8f	cc-pV5Z*	38.8
8s8p8d8f	cc-pV6Z*	35.4
8s8p8d8f	cc-pV5Z*	38.8
5s5p5d5f	cc-pV5Z*	38.8

^a The He—He is 2.3 Å, and the FGH tunneling splitting is 42.1 cm⁻¹.

^b The basis function center positions are optimized at the CCSD/aug-cc-pVTZ level of theory. The indicated protonic and electronic basis sets are used on the proton basis function centers. The aug-cc-pVTZ electronic basis set is used on He. No electronic active space and a full protonic active space are used.

Table S6. FHF⁻ Tunneling Splittings (in cm⁻¹) Computed with NEO-MR-SD_{en}CI with Varying Protonic Basis Sets^a

Protonic Basis Set	NEO-MR-SD _{en} CI ^b
8s8p8d	23.8
8s8p8d8f	27.5
5s5p5d5f5g	28.9

^a The F—F is 2.66 Å, and the FGH tunneling splitting is 26.7 cm⁻¹.

^b The basis function center positions are optimized at the CCSD/aug-cc-pVTZ level of theory. The indicated protonic basis set and the cc-pV5Z* electronic basis sets are used on the proton basis function centers. The aug-cc-pVTZ electronic basis set is used on F. A (2e,2o) electronic active space and a full protonic active space are used.

3 Electron Density

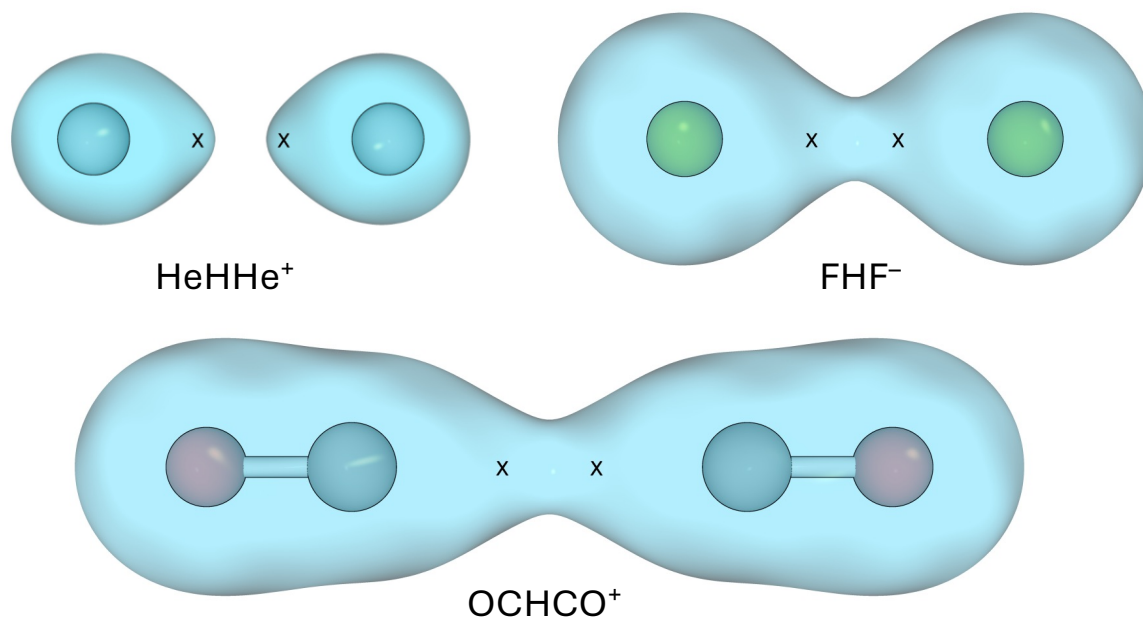


Figure S1. Electronic density of the ground state for HeHHe⁺, OCHCO⁺, and FHF⁻. The isovalue of the electronic density is 0.04 e Bohr⁻³ for all systems. The proton basis function center positions are indicated with an "X".

4 Electronic Active Spaces

Protonic orbitals are not shown, as a full protonic active space was used.

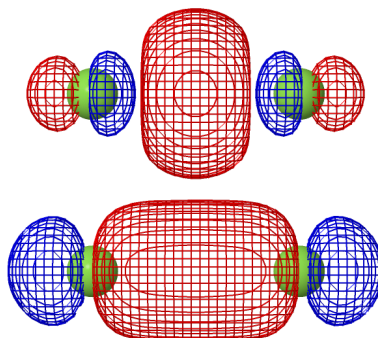


Figure S2. Electronic orbitals in the FHF^- active space.

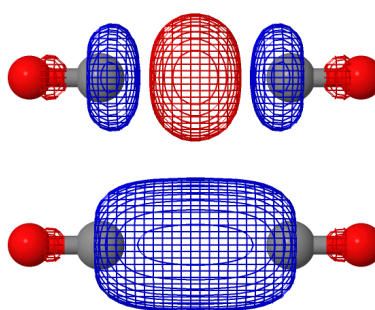


Figure S3. Electronic orbitals in the OCHCO^+ active space.

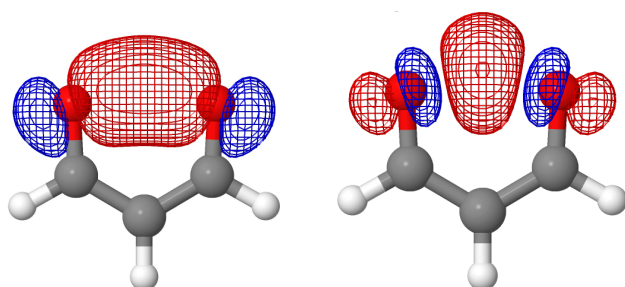


Figure S4. Electronic orbitals in the malonaldehyde active space.

5 OCHCO⁺ and FHF⁻ Protonic Densities

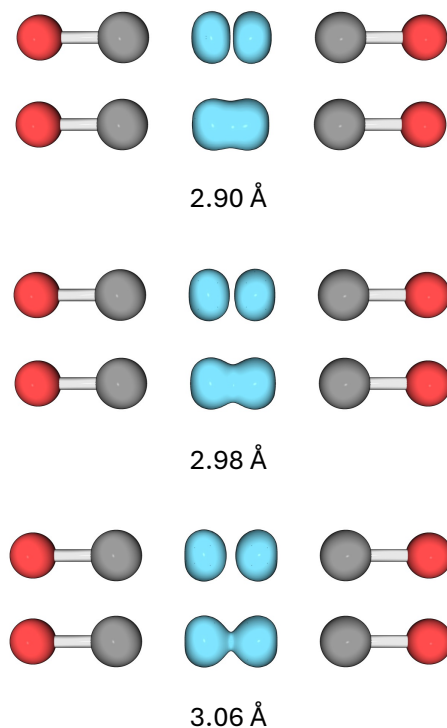


Figure S5. NEO-MR-SD_{en}CI protonic densities for OCHCO⁺ at the indicated C—C distances. The C atoms are shown in gray, the O atoms are shown in red, and the proton densities are shown in cyan with an isovalue of 0.04 e Bohr⁻³.

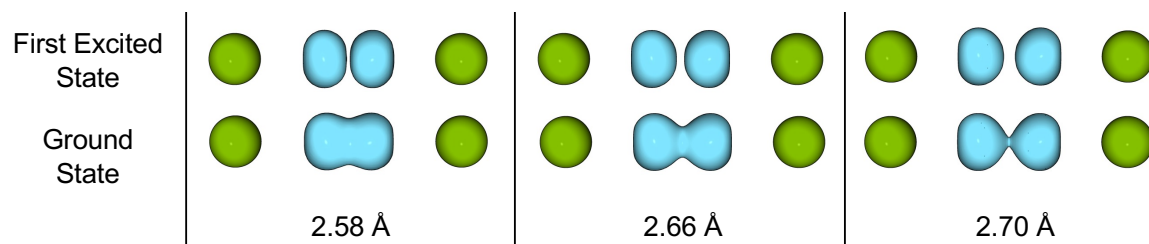


Figure S6. NEO-MR-SD_{en}CI protonic densities for FHF⁻ at the indicated F—F distances. The F atoms are shown in green, and the proton densities are shown in cyan with an isovalue of 0.04 e Bohr⁻³.

6 Coordinates

The geometries used in this work are provided below. These geometries include the optimized basis function center positions. The ghost centers are denoted with "GH". All units are in angstroms.

6.1 HeHHe⁺

He—He distance 2.2 Å

He	0.00000000	0.00000000	-1.10000000
He	0.00000000	0.00000000	1.10000000
H	0.00000000	0.00000000	-0.26938269
GH	0.00000000	0.00000000	0.26938269

He—He distance 2.25 Å

He	0.00000000	0.00000000	-1.12500000
He	0.00000000	0.00000000	1.12500000
H	0.00000000	0.00000000	-0.30370531
GH	0.00000000	0.00000000	0.30370531

He—He distance 2.3 Å

He	0.00000000	0.00000000	-1.15000000
He	0.00000000	0.00000000	1.15000000
H	0.00000000	0.00000000	-0.33611937
GH	0.00000000	0.00000000	0.33611937

He—He distance 2.35 Å

He	0.00000000	0.00000000	-1.17500000
He	0.00000000	0.00000000	1.17500000
H	0.00000000	0.00000000	-0.36711178
GH	0.00000000	0.00000000	0.36711178

He—He distance 2.4 Å

He	0.00000000	0.00000000	-1.12000000
He	0.00000000	0.00000000	1.12000000
H	0.00000000	0.00000000	-0.39618688
GH	0.00000000	0.00000000	0.39618688

6.2 FHF⁻

F—F distance 2.54 Å

F	0.00000000	0.00000000	-1.27000000
F	0.00000000	0.00000000	1.27000000
H	0.00000000	0.00000000	-0.25404100
GH	0.00000000	0.00000000	0.25404100

F—F distance 2.58 Å

F	0.00000000	0.00000000	-1.29000000
F	0.00000000	0.00000000	1.29000000
H	0.00000000	0.00000000	-0.28330200
GH	0.00000000	0.00000000	0.28330200

F—F distance 2.62 Å

F	0.00000000	0.00000000	-1.31000000
F	0.00000000	0.00000000	1.31000000
H	0.00000000	0.00000000	-0.31109700
GH	0.00000000	0.00000000	0.31109700

F—F distance 2.66 Å

F	0.00000000	0.00000000	-1.33000000
F	0.00000000	0.00000000	1.33000000
H	0.00000000	0.00000000	-0.33774000
GH	0.00000000	0.00000000	0.33774000

F—F distance 2.70 Å

F	0.00000000	0.00000000	-1.35000000
F	0.00000000	0.00000000	1.35000000
H	0.00000000	0.00000000	-0.36360540
GH	0.00000000	0.00000000	0.36360540

F—F distance 2.74 Å

F	0.00000000	0.00000000	-1.37000000
F	0.00000000	0.00000000	1.37000000
H	0.00000000	0.00000000	-0.38852230
GH	0.00000000	0.00000000	0.38852230

6.3 OCHCO⁺

C—C distance 2.90 Å

O	0.00000000	0.00000000	-2.56025300
O	0.00000000	0.00000000	2.56025300
C	0.00000000	0.00000000	-1.45000000
C	0.00000000	0.00000000	1.45000000
H	0.00000000	0.00000000	-0.28015112
GH	0.00000000	0.00000000	0.28015112

C—C distance 2.94 Å

O	0.00000000	0.00000000	-2.58025300
O	0.00000000	0.00000000	2.58025300
C	0.00000000	0.00000000	-1.47000000
C	0.00000000	0.00000000	1.47000000
H	0.00000000	0.00000000	-0.30792752
GH	0.00000000	0.00000000	0.30792752

C—C distance 2.98 Å

O	0.00000000	0.00000000	-2.60025300
O	0.00000000	0.00000000	2.60025300
C	0.00000000	0.00000000	-1.49000000
C	0.00000000	0.00000000	1.49000000
H	0.00000000	0.00000000	-0.33383391
GH	0.00000000	0.00000000	0.33383391

C—C distance 3.02 Å

O	0.00000000	0.00000000	-2.62025300
O	0.00000000	0.00000000	2.62025300
C	0.00000000	0.00000000	-1.51000000
C	0.00000000	0.00000000	1.51000000
H	0.00000000	0.00000000	-0.35990776
GH	0.00000000	0.00000000	0.35990776

C—C distance 3.06 Å

O	0.00000000	0.00000000	-2.64025300
O	0.00000000	0.00000000	2.64025300
C	0.00000000	0.00000000	-1.53000000
C	0.00000000	0.00000000	1.53000000
H	0.00000000	0.00000000	-0.38528111
GH	0.00000000	0.00000000	0.38528111

C—C distance 3.10 Å

O	0.00000000	0.00000000	-2.66025300
O	0.00000000	0.00000000	2.66025300
C	0.00000000	0.00000000	-1.55000000
C	0.00000000	0.00000000	1.55000000
H	0.00000000	0.00000000	-0.40942460
GH	0.00000000	0.00000000	0.40942460

6.4 Malondaldehyde

O—O distance 2.55 Å

GH	-0.32439202	-0.32293234	0.00000000
H	0.32439202	-0.32293234	0.00000000
O	-1.27500000	0.00000000	0.00000000
O	1.27500000	0.00000000	0.00000000
C	-1.20470340	1.27297710	0.00000000
C	1.20470340	1.27297710	0.00000000
C	0.00000000	1.98626359	0.00000000
H	0.00000000	3.06283598	0.00000000
H	-2.15371942	1.80885491	0.00000000
H	2.15371942	1.80885491	0.00000000

O—O distance 2.62 Å

GH	-0.37316353	-0.34058562	0.00000000
H	0.37316353	-0.34058562	0.00000000
O	-1.30832137	0.00507320	0.00000000
O	1.30832137	0.00507320	0.00000000
C	-1.21275237	1.27683755	0.00000000
C	1.21275237	1.27683755	0.00000000
C	0.00000000	1.97816598	0.00000000
H	0.00000000	3.05507430	0.00000000
H	-2.15184510	1.83064627	0.00000000
H	2.15184510	1.83064627	0.00000000